J. Fluid Mech. (1968), *vol.* 32, *part* 1, *pp.* 69–96
Printed in Great Britain

The unstable thermal interface

By J. W. ELDER
Department of Applied Mathematics and Theoretical Physics, Cambridge

(Received 27 February 1967 and in revised form 17 October 1967)

The motion which develops in a deep layer of a viscous, thermally conducting fluid initially hot below and cold above some horizontal plane, so that the system is gravitationally unstable, is studied by laboratory and numerical experiments. Three cases are considered: (i) the flow which occurs in a porous medium when the interface is the lower boundary of the system; (ii) a similar study in a viscous fluid; (iii) an interface distant from the confining horizontal boundaries, in a viscous fluid. In all cases the initial development of the flow—assuming an initial source of noise, for example as temperature fluctuations—occurs within the thermal interface between the hot and cold fluid. The scale of the motion is set by the thickness of the interface.

The development of the disturbances in the interface involves: a period of local thickening and induced, damped motions in which the diffusion of heat and vorticity dominate; a period of gestation, involving rapid amplification, with the disturbance imbedded in the interface and diminishing importance of the role of diffusion of heat; a period of emergence of the disturbances from the interface, during which the accelerations are sufficiently rapid for molecular processes to be unimportant, entrainment being the dominant process, and the gravitational energy accumulated locally in the interface is largely removed; and finally a period of adjustment of the large eddies. The amplification process is adequately described by the linearized equations of motion.

1. Introduction

The motion of a layer which is unstably stratified is an archetypal problem in the theory of flows driven by buoyancy forces. There are two classic problems of this type, each of which presents an extreme situation. The first case is the Rayleigh–Taylor problem, the simplest version of which considers two semi-infinite layers of fluid between which there is a sharp interface and across which diffusion of momentum and density is ignored. If the upper fluid is denser than the lower fluid the situation is clearly unconditionally unstable. The second case is the Bénard–Rayleigh problem, in which the 'interface' is a broad region of more or less uniform unstable density gradient, more or less confined above and below. The essential feature of this flow is the combined stabilizing action of the diffusion of *both* momentum and density. Between these two extreme situations there is a wide class of flows. The problem which has motivated this study is one of them.

Consider, for example, the situation sketched in figure 1, a layer of fluid made unstable by heating a lower portion. Let us allow diffusion of both momentum

and density. For a time the initially sharp density interface will spread by molecular diffusion but there is the possibility once the interfacial region becomes sufficiently thick, that any disturbances which are present will grow in the interfacial region. We would then have a Bénard–Rayleigh type of problem. On the other hand, the layer as a whole is unstable and it is inevitable that the interface will ultimately become disrupted. We would then have a Rayleigh–Taylor type of problem. It is of interest to investigate how these two processes are linked together. As we shall see, in the development of the flows discussed below, there is a progressive change from dominance of the flow by diffusion of both momentum and density and then a loss of importance of first, diffusion of density and secondly of momentum till entrainment processes become dominant and the interface is disrupted.

The object of our study is the growth of disturbances in a thin thermal layer. If the layer is attached to a boundary I shall refer to it as the *proto-sublayer*. The experimental and numerical results are collected in §§4–6, followed by a rather heuristic analysis and assessment of the results in §§7 and 8. Finally §9 gives a discussion of the role of the thermal sublayer in thermal turbulence in the light of the present results.

2. Statement of the problem

Let us consider the situation sketched in figure 1, a body of fluid of depth H bounded above and below by horizontal, rigid, conducting walls and bounded on the sides by vertical, rigid, insulating walls a distance lH apart where $l > 1$. The fluid is at a uniform temperature T_0 and is at rest. At time $t = 0$ a lower portion of the fluid of depth hH has its temperature increased to $T_0 + \Delta T(1+\epsilon)$, where ϵ is a random function of position and time and the lower surface $z = 0$ is subsequently held, in general, at the temperature $T_0 + \Delta T(1+\epsilon(x,0,t))$. We restrict the investigation to the development of the consequent two-dimensional motions in which the velocities are confined to the (x,z)-plane.

Two closely related problems are discussed. The first is for flow in a porous medium or Hele–Shaw cell; the second is in a viscous fluid. In a porous medium vorticity is generated by the horizontal gradient of the buoyancy force and heat is transferred by diffusion and advection. A viscous fluid allows the additional processes of diffusion and advection of vorticity.

In a porous medium, inspection of the field equations show that the flow is specified by the aspect ratios, l, h and

$$k\gamma g\Delta T/\nu, \quad \kappa, \quad H,$$

where k is the permeability, γ the coefficient of cubical expansion, g the gravitational acceleration, ν the kinematic viscosity, and κ is the thermal diffusivity of the fluid†. Hence, since these quantities involve only length and time the system is, in addition to the aspect ratios, defined by the single parameter

$$A = k\gamma g\Delta TH/\kappa\nu \quad \text{(Rayleigh number)}.$$

† Since all the experiments for this case were in a Hele–Shaw cell rather than in a porous medium, κ is strictly the thermal diffusivity of the fluid, which is not the case in a porous medium.

It will be convenient to chose units of length, velocity and temperature: H, κ/H, ΔT so that subsequently, unless stated to the contrary, all quantities are dimensionless. We shall also often refer to the horizontally averaged properties of the sublayer in terms of its thickness δ ($\approx 2\sqrt{t}$ for most of the present study), the dimensionless heat transfer coefficient N, the Nusselt number, and the horizontally averaged vertical temperature gradient $\beta = \beta(z,t)$. The subscripts c, ∞ refer to the critical state in which a disturbance can first grow and to the state as $t \to \infty$.

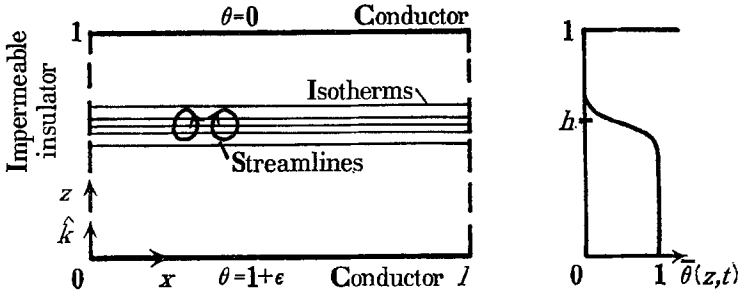

FIGURE 1. Diagram of the container, the cartesian co-ordinate system and typical undisturbed vertical temperature profile at a time $t > 0$. Length unit H, the layer depth.

The field equations (Wooding 1957) for the temperature θ and streamfunction ψ for two-dimensional motion in a porous medium, in dimensionless form, reduce to

$$\omega = A\theta_x, \tag{1a}$$

$$\nabla^2\psi = \omega, \tag{1b}$$

$$\frac{\partial\theta}{\partial t} = \nabla^2\theta - \partial(\psi,\theta), \tag{1c}$$

where the velocity $\mathbf{q} = (-\psi_z, \psi_x)$ and the vorticity $\boldsymbol{\omega} = -\hat{\jmath}\omega$ where $\hat{\jmath}$ is unit vector parallel to the y-axis. The boundary conditions are: $\psi = 0$ on the walls; $\theta = 1+\epsilon(x,0,t)$, 0 on $z = 0, 1$; and $\theta_x = 0$ on $x = 0, 1$. The initial conditions are: $\psi = 0$; $\theta = 0$ for $z > h$; $\theta = 1+\epsilon(x,z,0)$ for $z \leqslant h$. Throughout, ϵ is a random function, with a white spectrum, of zero mean and r.m.s. amplitude ϵ'. Note that except in § 6 we shall study only the case $h = 0$.

In a viscous fluid the system is similarly defined by

$$A^* = \gamma g \Delta T H^3/\kappa\nu \quad \text{(Rayleigh number)},$$

$$\sigma = \nu/\kappa \quad \text{(Prandtl number)},$$

and the field equations are the same as (1) except that the vorticity equation (1a) becomes

$$\frac{\partial\omega}{\partial t} = \sigma\nabla^2\omega + \sigma A^*\theta_x - \partial(\psi,\omega). \tag{2}$$

We note that here, while we have the additional processes of diffusion and advection of vorticity, if σ is sufficiently large the only extra process is the diffusion of vorticity.

In order to see the relation of this to previous studies consider for the moment the gross features of the development for the case $h = 0$. Initially all the ambient fluid is at temperature zero, but after a dimensionless time† of order $1/N_\infty$ the mean temperature of nearly all the fluid is at a temperature near 0·5. The development of such a flow is summarized in figure 2 which shows a typical gross feature of the flow, ψ_m, the maximum absolute value of ψ over the flow space as a function of time. For the period of order $10^2 A^{*-\frac{2}{3}}$ there is rapid increase of the mass transport, after which the system approaches statistical equilibrium. The wiggly record with values of ψ_m ranging of order $\pm 20\,\%$ about its temporal mean is then maintained. The flow as $t \to \infty$ is characterized by an intermittently unstable sublayer and an interior dominated by eddies of length scale H. Previous

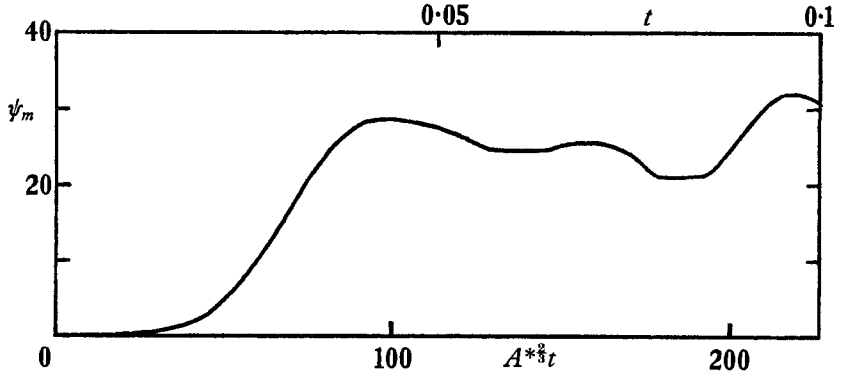

FIGURE 2. Development of the flows as a whole. Free convection in a viscous fluid at $A^* = 10^5$, $\sigma = 1$, $l = 2$, $\epsilon' = 0{\cdot}2$. Maximum absolute value of the streamfunction $\psi_m(t)$.

numerical simulations (e.g. Deardroff & Willis 1965; Elder 1967*a*, *b*) of these flows shows, provided temperature fluctuations are maintained at the walls, that the gross features of the flow, for example, the development of the mean temperature and the r.m.s. temperature fluctuations, are in reasonable agreement with experiment. These studies have dealt largely with this latter statistically steady régime. Here we wish to concentrate attention on the early stages of the development in which the proto-sublayer is completely dominant.

In thermal turbulence we know from experiment that the heat transferred across the layer for a given ΔT is independent of the spacing of the plates as are the gross features of the sublayer. We expect here, too, that the early stages of development of the proto-sublayer will be independent of H. It may therefore seem silly to choose H as a length scale. In practice, however, both numerically and in the laboratory the depth of fluid is finite. But more important, the choice is very convenient because it provides a check on our predictions since in dimensional form they must be independent of H. For example, the system of equations (1*b*, *c*) and (2) have the same form under a change of units of length and time to δ and δ^2 except that in the buoyancy term A^* is replaced by $A^*\delta^3$. We can choose δ such that $\delta \propto A^{*-\frac{1}{3}}$. The corresponding time unit is $A^{*-\frac{2}{3}}$. This is consistent with

† $N_\infty \approx 0{\cdot}08 A^{*\frac{1}{3}}$ is the Nusselt number in the statistically steady state realized as $t \to \infty$.

our expectation that the layer will become unstable when $A^*\delta^3 = A_c^* =$ constant and the time of onset of amplification $t_c \propto \delta^2$, and horizontal wavelength λ at the first appearance of motion at time t_1 is given by $\lambda^2 \propto t_1$.

3. Experimental results in a Hele-Shaw cell

The experiments in Hele-Shaw cells have covered the range $A = 0$–2000, $l = 1$–10. These experiments are very convenient when the growing disturbances have become large, but a study of the initial development is very difficult. Hence most of the detailed studies have been made numerically. The techniques and apparatus used here are closely similar to those of a previous study (Elder 1967*c*). The Hele-Shaw cells were made of perspex and the silicon oil MS 200/100 cs was used. Two geometries were used: (i) plate spacing, $a = 4$ mm, $H = 4$ cm; (ii) $a = 1$ mm, $H = 6$ cm. Note that the permeability $k = \frac{1}{12}a^2$.

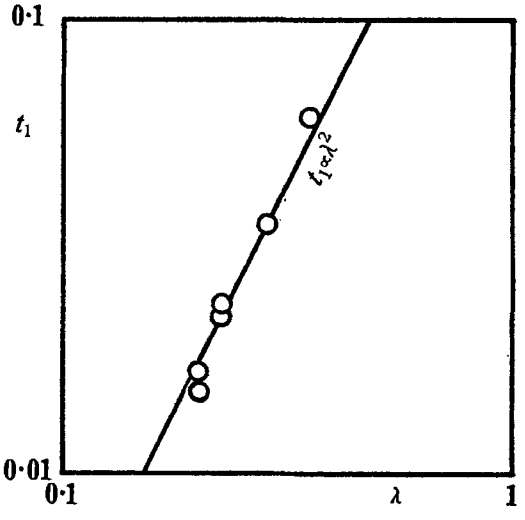

FIGURE 5. Wavelength λ at time of first appearance t_1 in a Hele-Shaw cell.

The gross features of the development to the statistically steady state are illustrated in the photographic sequence of figure 3, plate 1, which shows a layer uniformly heated from below at $A = 250$. The first striking development is the array of blobs rapidly growing above the lower surface. This is followed by the gradual appearance of a large-scale cellular pattern of ever changing eddies. This latter stage is not our present concern. The second photographic sequence, shown in figure 4, plate 2, is a close up of the proto-sublayer showing the early development of the eddies embedded in the layer.

Observation of the proto-sublayer clearly demonstrates that the disturbances remain embedded in the proto-sublayer until they reach a finite amplitude. During this time the remaining ambient fluid is still very nearly at rest. The scale of the flow is therefore dominated by the scale δ of the proto-sublayer. This is the essential fact revealed by this study. Quantitative evidence for this statement is presented in figure 5, which shows the mean horizontal wavelength λ

of the disturbance pattern as a function of the time of first appearance of motion t_1. The wavelength was determined by counting the total number of eddies n and evaluating $\lambda = l/n$. The time t_1 is rather difficult to determine and there is no doubt that the eddying motions are already well established by the time they are noticed. Different values of t_1 are arranged by repeating the experiment at different values of ΔT. The data show, within the rather poor experimental accuracy, reasonable correlation with the expected relation $\lambda^2/t_1 \approx$ constant. The correlation of figure 5 does not involve ν. This is very nice since it avoids the complicating factor of ν being a function of temperature which needs considerations not of immediate concern in this paper. An investigation of the role of $\nu(T)$ in several convective systems is in progress but a single example should serve as a warning to the reader. Experiments in a viscous fluid with large values of ΔT using medicinal paraffin, for which $\nu \propto T^{-\frac{3}{2}}$ (T in °C), show that the time t_1 of visible onset of motion, which is proportional to $\Delta T^{-\frac{3}{2}}$ for an ideal fluid, is more nearly like ΔT^{-2}, which is the result of an ideal fluid in a porous medium.

These experiments reveal the same qualitative features as those found in the experiments of Spangenberg & Rowland (1961) and Foster (1965*a*), both of whom studied a layer of water cooling from above. In spite of their cruder visualization techniques they showed that in deep layers the process was independent of H and that the critical proto-sublayer Rayleigh number was similar to that given by the Rayleigh stability theory.

4. The proto-sublayer in a porous medium: numerical results

The numerical experiments with the simulated flows in a porous medium have partially covered the range: $A = 0$–1600; $l = 1$–5; $\epsilon' = 0$–$0{\cdot}5$. Solutions were always possible provided the smallest scale to be represented—which is δ, the sublayer thickness—was not less than 1 mesh interval. The results will be merely presented here and discussed in §7. The finite difference technique used is identical to that previously used by the author (Elder 1967*c*). Poisson's equation is solved by a slightly modified successive over-relaxation procedure. The time step is the so-called Eulerian one, a forward difference in time. The finite difference application of the side wall boundary condition $\theta_x = 0$ was performed in a time-dependent manner. The mesh spacing was generally 1/40, but sufficiently different choices of it and the time step indicated that the solutions are reliable to within a few per cent.

If either the Rayleigh number is small (< 40), or the horizontally averaged vertical temperature gradient $\beta = \beta(z, t)$ is zero, only a weak induced motion is possible. Further, if the only source of temperature fluctuations is on one of the horizontal walls, the induced motion is confined to a region near the wall. For example, the flow of figure 6 is for the case in which $\theta = \epsilon(x, t)$ on $z = 0$. As we shall see below this is the type of motion generated immediately after $t = 0$ regardless of the value of A.

Provided A is sufficiently greater than the critical Rayleigh number $A_c = 4\pi^2$ (Lapwood 1948), for the proto-sublayer thickness δ to be much less than unity, the proto-sublayer grows as if it were at the bottom of an infinitely deep layer of

fluid. Figures 7–9 show the state of the proto-sublayer at successive times for $A = 200, 400, 800$ for which $N_\infty \approx 5, 10, 20$. At the earlier times we see a horizontally uniform thermal layer growing into the fluid, embedded in which are an array of eddies of roughly the same size and amplitude. At the later times, however, the thermal layer has become grossly distorted where portions of it are

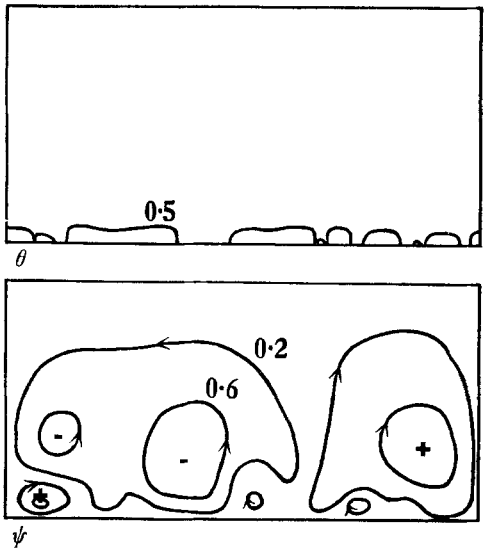

FIGURE 6. Induced motion. Contours of $\psi/\psi_m = 0{\cdot}2, 0{\cdot}6$ where $\psi_m = 4 \times 10^{-6}$ for $A = 1$, $\epsilon' = 0{\cdot}4$, $t = 0{\cdot}01$.

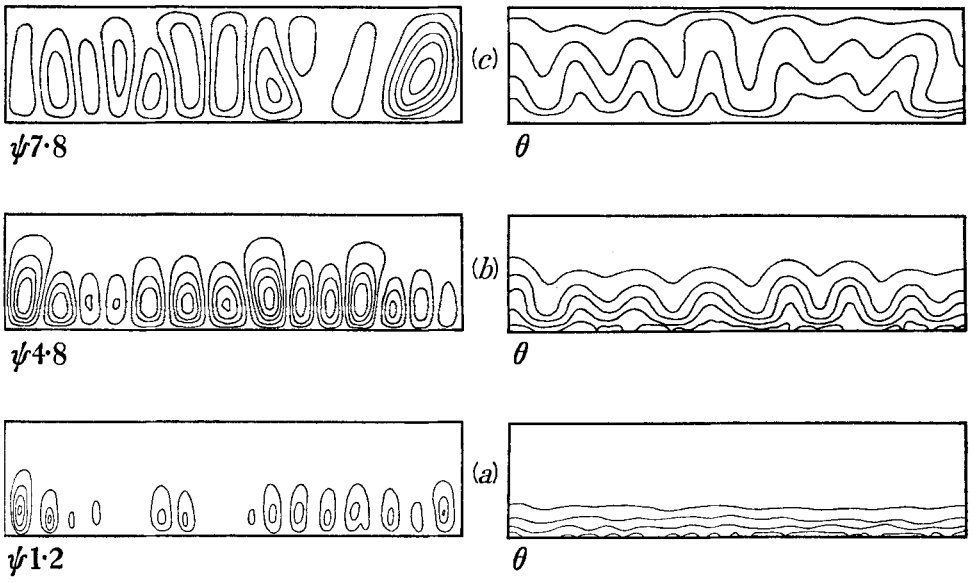

FIGURE 7. Time development of proto-sublayer in a porous medium: $A = 200$, $l = 4$, at times: (*a*) 2×10^{-2}, (*b*) 4×10^{-2}, (*c*) 8×10^{-2}. In this and subsequent figures the contours are at intervals $-1(0{\cdot}2)1$ times the scale value of the field variable which is 1 for θ and for ψ is the value written on the figure.

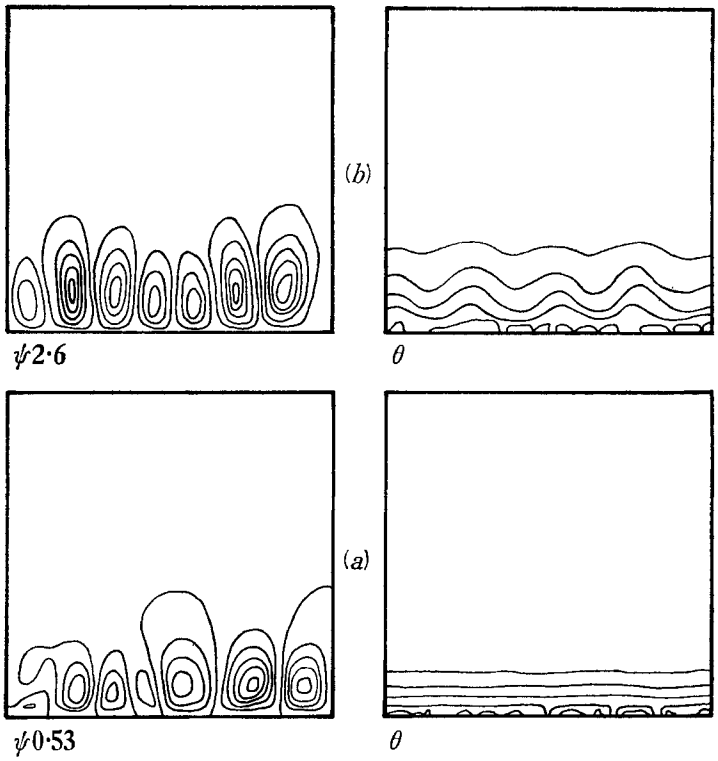

FIGURE 8. As for figure 7: $A = 400$, $l = 1$. (a) $t = 5 \times 10^{-3}$, (b) $t = 10^{-2}$.

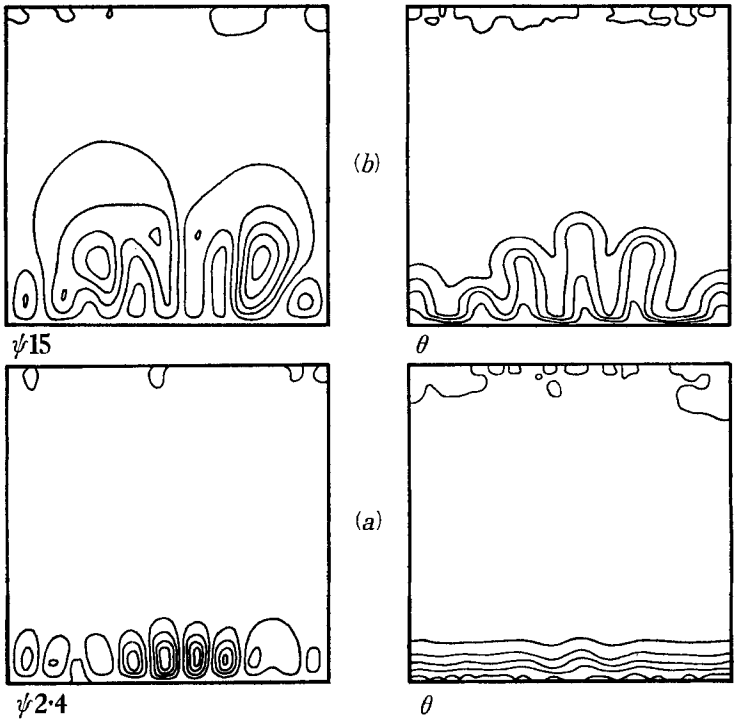

FIGURE 9. As for figure 7: $A = 800$, $l = 1$. (a) $t = 2{\cdot}5 \times 10^{-3}$, (b) $t = 5 \times 10^{-3}$. In this example thermal noise is allowed on both horizontal boundaries but the initial temperature of the fluid body is zero.

rising above the wall. The eddies are no longer embedded in the layer, and rapidly become separate entities. The geometry of figure 7 is the same as that of the photographic sequence of figure 3. The two flows can be roughly compared by noting that in the numerical study $t_c \approx 10^{-2}$ (more precisely $0{\cdot}88 \times 10^{-2}$) so that figure 7 shows the flow at $t \approx (2, 4, 8)t_c$, while for the laboratory study $t_c \approx 50$ sec so that the corresponding times are 100, 200, 400 sec. An exact correspondence is not to be expected since the two noise sources are not identical. The flows at the other values of A, apart from a pronounced contraction of time scale with increasing A show essentially the same development. In passing, it is worth noting, especially at the higher values of A, the tendency for amalgamation of eddies (see figure 9*b*). This tendency, which is also seen in the laboratory experiments, represents a broadening of the spatial spectrum of the velocity field to *lower* wave-numbers. Finally we note that during the proto-sublayer stage the initially larger eddies remain the larger eddies.

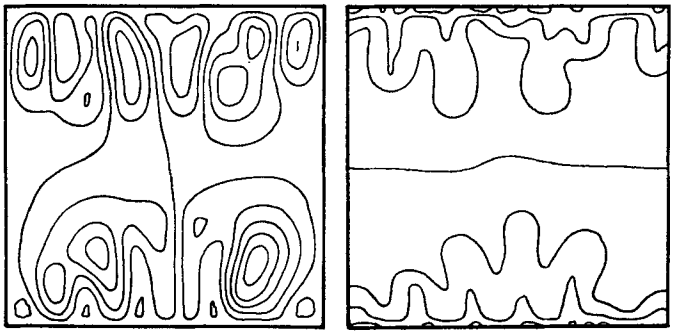

FIGURE 10. As for figure 9 but with the initial temperature of the fluid body at 0·5 and hence proto-sublayers on both $z = 0$ and $z = 1$ illustrating the independent growth of the two layers and the detailed difference of response to different sequences of noise impulses. $A = 1600$, $t = 5 \times 10^{-3}$.

That the fluid depth does not affect the initial development of the proto-layer is illustrated in figure 10. This shows a case in which the ambient fluid is at $\theta = \frac{1}{2}$ and $\theta = \epsilon_1(x, t)$ on $z = 1$ and $\theta = 1 + \epsilon_0(x, t)$ on $z = 0$ where ϵ_1 and ϵ_0 are obtained from different portions of the same array of bounded random numbers. Proto-sublayers grow independently for a period of order $1/A$. This example also illustrates two simple points. First, we must remember to compare sublayers by means of the Rayleigh number based on the temperature difference *across* the sublayer (note below, figure 12). Secondly, we see the difference between the details of the development of the two sublayers arising from two incoherent though otherwise equal noise sources.

A summary of this development is presented in figure 11 which shows a typical gross parameter of the flow $\psi_m(t)$, the maximum absolute value of ψ over the mesh, as a function of time. We recognize three periods in the development: (i) gestation, (ii) growth, and (iii) flight. The gestation period, which in the example of figure 9 occupies a time interval t_c of $0{\cdot}8 \times 10^{-3}$, involves two processes: the rapid establishment of an induced flow; followed by a period of quasi-

equilibrium. After a time of roughly $2t_c$ the growth rate, within the numerical error, is closely exponential. The final exponential growth rates $n = \partial(\log \psi_m)/\partial t$, determined from such curves, are shown in figure 12. They fairly closely satisfy $n/A^2 = \text{constant}$, again a result independent of H.

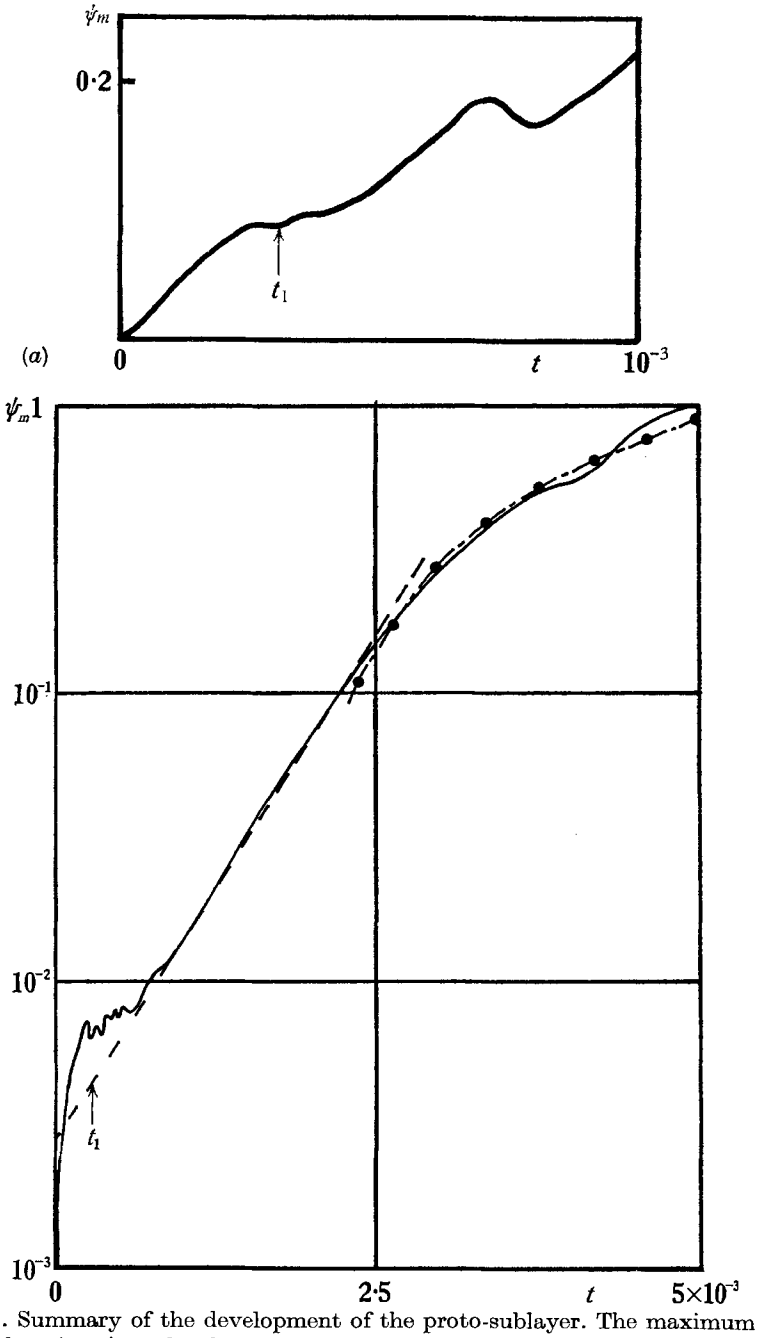

FIGURE 11. Summary of the development of the proto-sublayer. The maximum value of the streamfunction $\psi_m(t)$ for the flow of figure 9, $A = 800$. (*a*) linear scales; (*b*) log-linear scales. ψ_m scaled to unity at $t = 5 \times 10^{-3}$; multiply by 15·5 to obtain actual values.

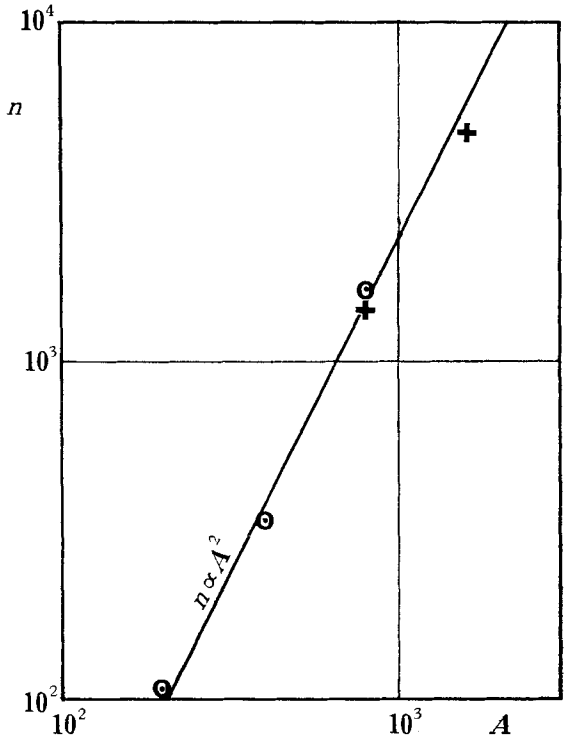

FIGURE 12. Exponential growth rate in a porous medium: $n = \partial(\log \psi_m)/\partial t$ as a function of A. Initial body fluid temperature: ⊙, $\theta = 0$; +, $\theta = 0{\cdot}5$, points plotted at $\frac{1}{2}A$.

5. The proto-sublayer in a viscous fluid: numerical results†

Numerical experiments on the proto-sublayer in a viscous fluid have partially explored the range $A^* = 0$–10^9, $l = 1$–5, $\epsilon' = 0$–$0{\cdot}5$, but have for the present purpose been restricted to $\sigma = 1$. The development of the proto-sublayer is shown in figures 13 and 14 at two successive times for $A^* = 10^6$, 10^7 for which $N_\infty \approx 10$, 20. These figures should be compared with figures 8 and 9 with which they are very similar. Figure 13 shows part of the interval of exponential growth during which the disturbances remain embedded in the growing thermal layer. Distortions of the temperature field begin to be noticeable at $t = 4 \times 10^{-3}$, in figure 13*b*. On the other hand, the data selected for figure 14 show the final period of growth and eruption. In this calculation the time step has purposely been chosen about as large as possible, without the solution diverging, to simulate the rather spotty temperature fields found in the laboratory in poorly controlled experiments where, in particular, ϵ' is large and variable. The gross development of the proto-sublayer is illustrated in figure 15, which should be compared with

† The only feature required in addition to the technique of §4 is the method of applying the boundary conditions on ω. We use the well-known method of stepping (2) forward in time only on the interior points and then evaluating ω on the walls from (1*b*) but with the operation written for the case of the normal derivate $\psi_n = 0$. These results are collected here for convenience; the reader may prefer to go directly to the discussion of §7 and refer to §§5 and 6 later, as required.

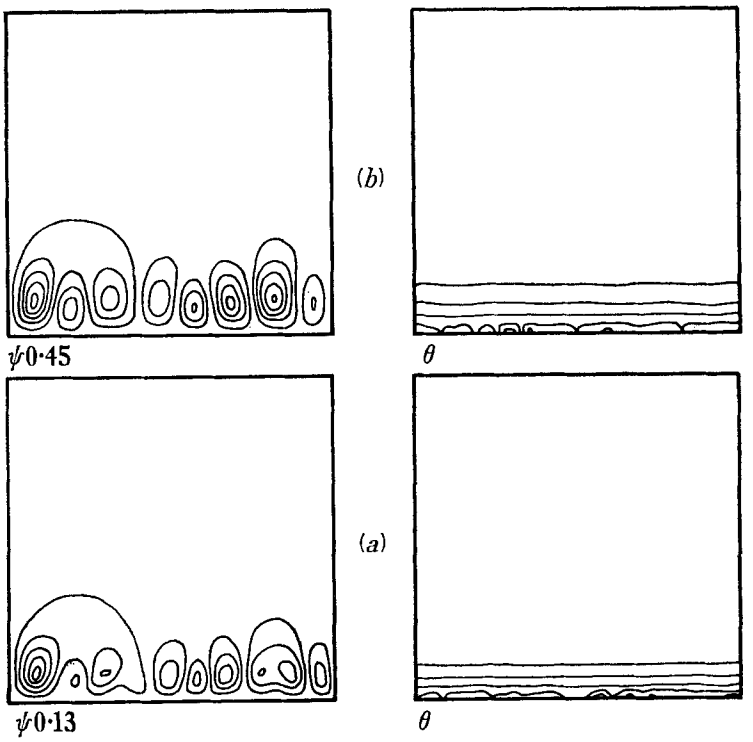

FIGURE 13. Time development of the proto-sublayer in a viscous fluid with $A = 10^6$; $\sigma = 1$. Streamfunction ψ, the temperature θ at times: (*a*) $t = 2 \times 10^{-3}$, (*b*) $t = 4 \times 10^{-3}$. Period of exponential growth.

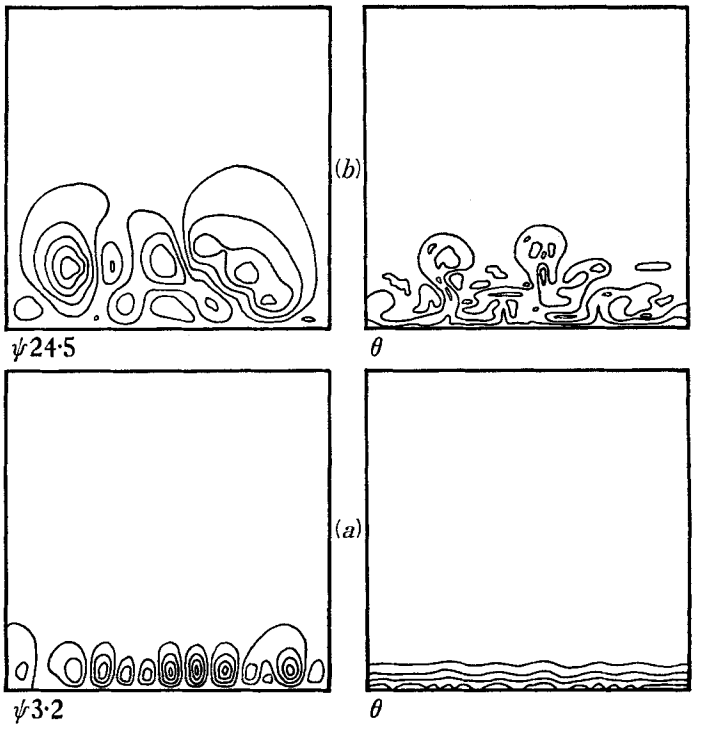

FIGURE 14. Time development of the proto-sublayer in a viscous fluid with $A = 10^7$; $\sigma = 1$. Streamfunction ψ and temperature θ at times: (*a*) $t = 10^{-3}$; (*b*) $t = 2 \times 10^{-3}$. Final

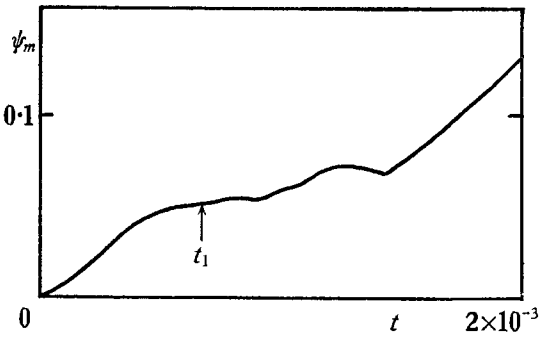

(*a*)

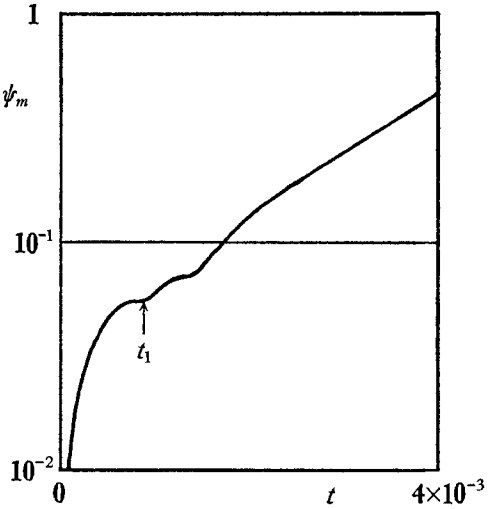

(*b*)

FIGURE 15. Summary of the development of the proto-sublayer in a viscous fluid at $A = 10^7$, $\sigma = 1$ as shown in figure 14. The maximum value of the streamfunction $\psi_m(t)$: (*a*) linear scales; (*b*) log-linear scales.

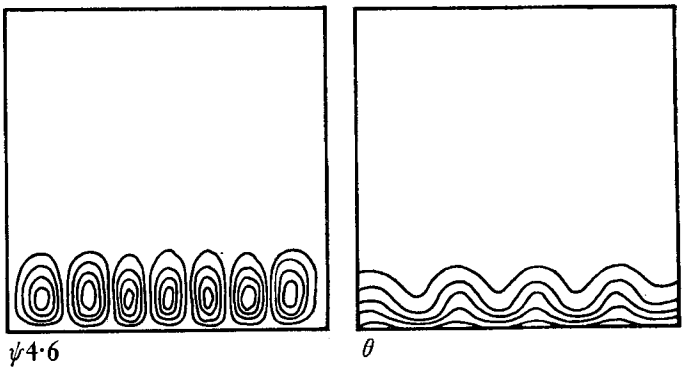

FIGURE 16. Growth of non-time varying disturbance with $\epsilon = 0{\cdot}1 \sin(4\pi x)$, $A = 10^6$, $t = 4\times10^{-3}$.

figure 11. The processes of advection and diffusion of vorticity do not seem to have made much qualitative difference!

A number of other experiments have been made to study crudely the role of the spatial spectrum of the temperature fluctuations specified on the boundary.

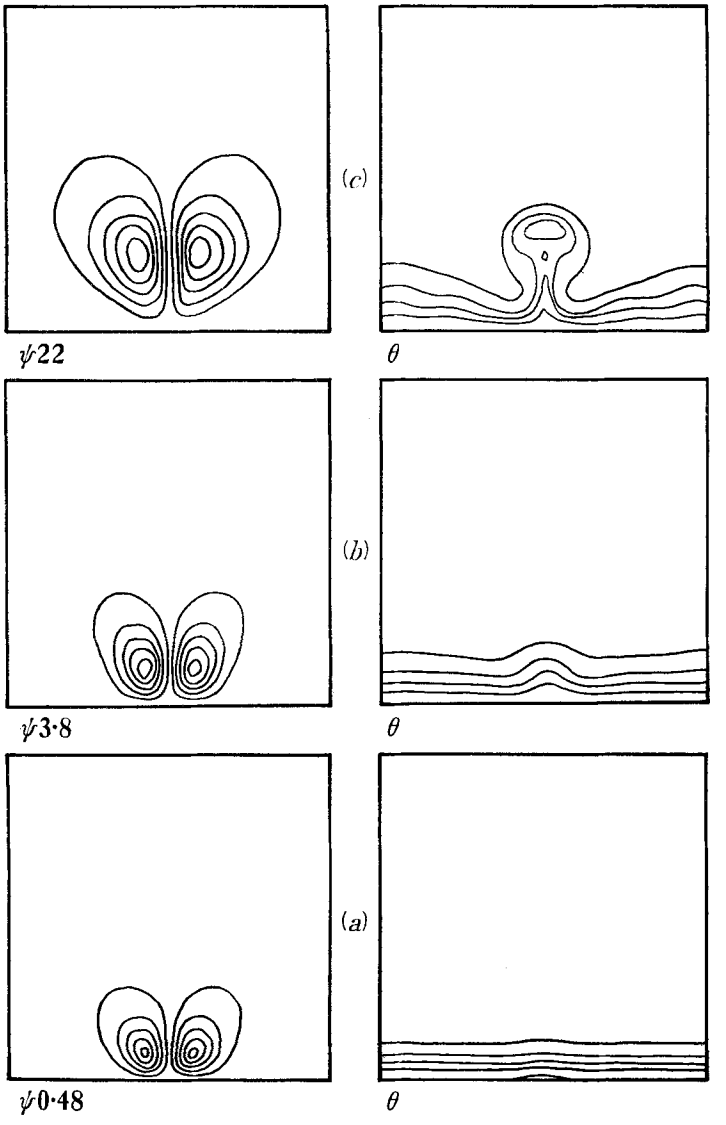

FIGURE 17. Growth of an individual blob at $A = 10^6$, $\sigma = 1$ showing the entrainment into the blob. Heater width 1/8, $\epsilon = 0{\cdot}1$: (*a*) $t = 2 \times 10^{-3}$; (*b*) $t = 4 \times 10^{-3}$; (*c*) 6×10^{-3}.

The data of figure 16 show the case $\epsilon \propto \sin kx$: a non-time varying spatial modulation of the temperature of the lower wall. The data of figure 17 show the case ϵ = constant over a small region of extent δ_c in the middle of the lower wall. Both of these 'fixed' sources lead to the same development and exponential growth rates as that of the random noise. The major difference between the flows

of figures 13, 16 and 17, which are all at $A = 10^6$, is in the greater disturbance amplitude. This is simply a consequence of the fact that the fastest growing disturbance has a length scale of order δ so that in effect the large content of ϵ in other scales, in the flow of figure 13, is filtered out. Throughout the numerical study we have mainly used $\epsilon' = 0{\cdot}2$, a rather large value. This choice is largely dictated by computer time since, although the growth rates are exponential, the time to grow to finite amplitude increases rapidly as ϵ' is reduced.

The flow of figure 17 leads to the production of an isolated blob and nicely shows the entrainment field about the rising blob. The blob has already lifted itself above the bottom surface at $t = 6 \times 10^3$ as shown in figure 17*c*.

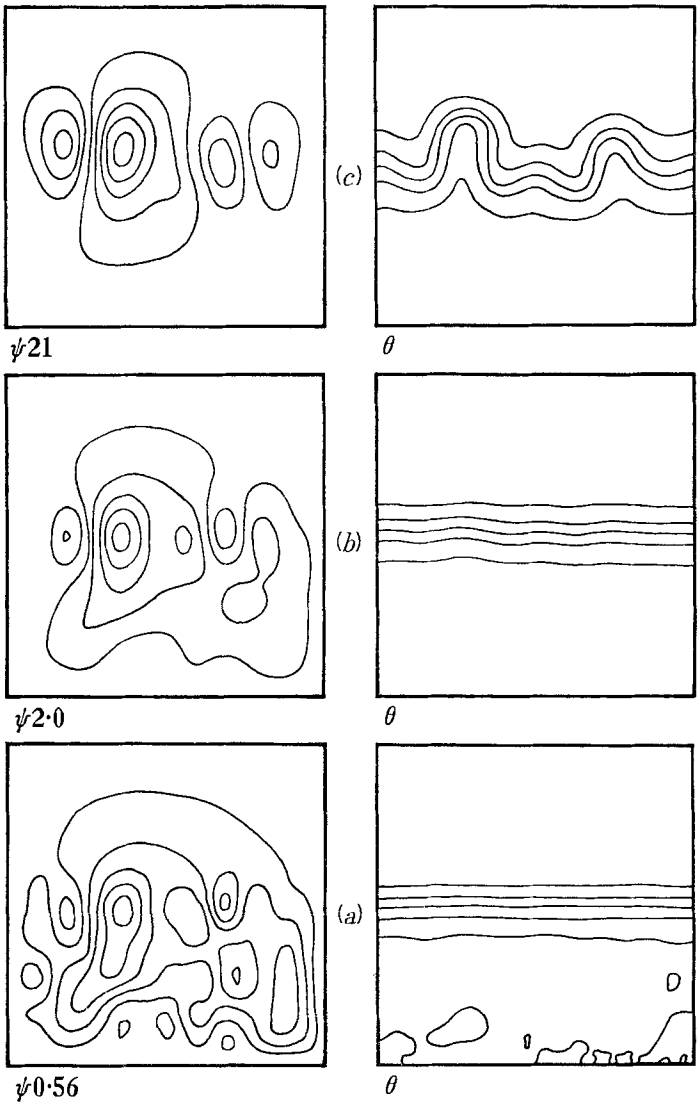

FIGURE 18. Time development of a free interface in a viscous fluid with $h = 0{\cdot}5$, $A = 10^6$, $\sigma = 1$. Streamfunction ψ and temperature θ at times: (*a*) $t = 10^{-3}$; (*b*) $t = 2 \times 10^{-3}$; (*c*) $t = 4 \times 10^{-3}$.

6. The isolated thermal interface in a viscous fluid: numerical results

In the course of trying to understand the mechanism that determines the initial distortions of the thermal layer and, in particular, what process sets the horizontal scale of the distortions it occurred to me that the problem had much in common with the Rayleigh–Taylor problem. Hence a number of numerical experiments were performed to clarify this idea. Here the thermal interface is placed away from the horizontal boundaries. A lower portion of depth h of the fluid layer is initially at rest at temperature $(1+\epsilon)$. We are interested in the horizontal scales of the subsequent motions at various h and expect qualitative similarity in the motions regardless of h and in particular with $h = 0$.

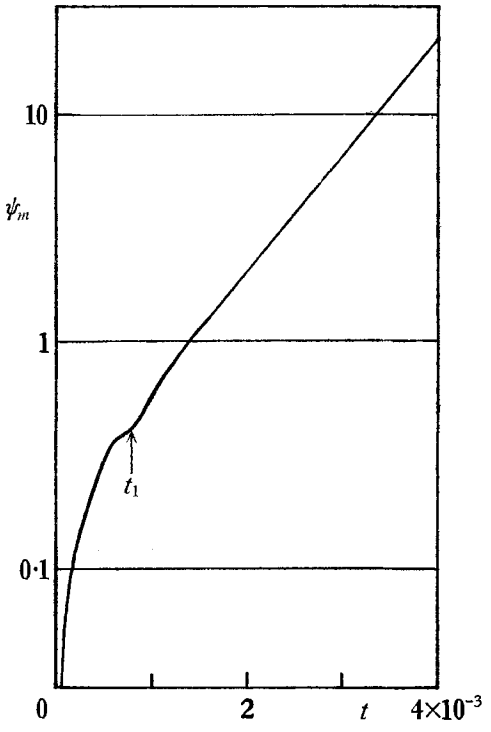

FIGURE 19. Summary of the development of the flow in a free interface at $A = 10^6$, $\sigma = 1$ as shown in figure 18; the maximum value of the streamfunction $\psi_m(t)$.

The development of a free interface in a viscous fluid is illustrated in figure 18 where $h = \frac{1}{2}$. Again we see the same development of the flow. At time $t = 10^{-3}$, as seen in figure 18*a*, the temperature distribution is only weakly disturbed. Effects arising from the initial noise in $h < \frac{1}{2}$ are still apparent. The induced flow is distributed throughout the lower layer but the maximum transports are already in the interface. By the time $t = 2 \times 10^{-3}$ in figure 18*b* the dominant growth in the interface is clearly seen and noticeable distortions of the temperature field are apparent. The flow at time $t = 4 \times 10^{-3}$ in figure 18*c* is sufficiently strong to produce violent distortions of the interface. We observe that the dominant

scales of motion have the scale of the interface. A summary of the development is shown in figure 19, which should be compared with figure 11.

Finally we show in figure 20, that the development is little influenced by the distance h of the interface from a wall unless $h < \delta_c$. The gross features of the three flows are very similar: the length scales are similar and there is little difference in the total transport ψ_m. The flow of figure 20*c* is somewhat different in so far as the plunging colder blobs are nearly impacting the lower surface, the constraint of which gives a little more regularity to the flow.

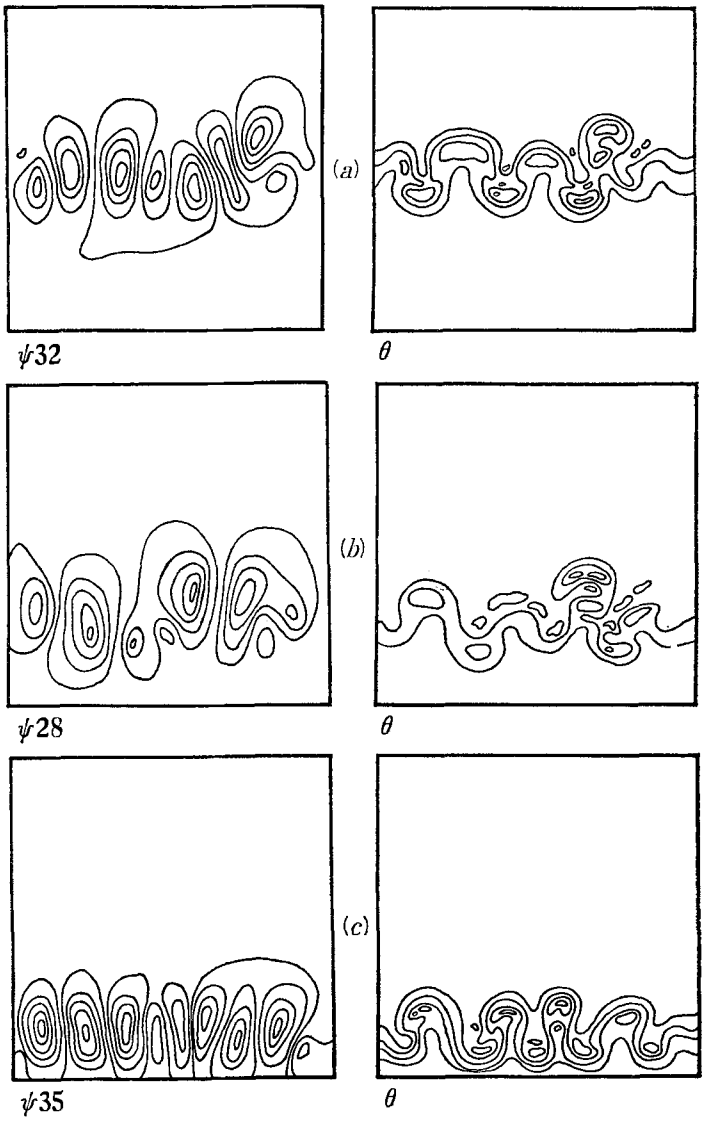

FIGURE 20. The role of the presence of the wall on the development of a free interface. The streamfunction ψ and temperature θ for $A = 10^7$, $\sigma = 1$, $\epsilon' = 0{\cdot}04$ at time $t = 10^{-3}$ for various interface positions: (*a*) $h = \frac{1}{2}$; (*b*) $h = \frac{1}{4}$; (*c*) $h = \frac{1}{8}$. Compare with figure 18 to see how the development is influenced by A. Compare with figure 14 where $h = 0$.

7. Analysis of the results

We have seen a few of the possible flows produced by unstable thermal interfaces. Now let us consider a number of simple theoretical models which will expose the main interactions in these flows. As we shall see, the amplification process can be adequately understood using the linearized equations of motion. This is perhaps no surprise, many of the deductions being readily adapted from, for example, the discussions in the tome by Chandrasekhar (1961). Only a sketch of the analysis is attempted here, the numerous details are a problem for the analyst. We discuss each of the flows in turn giving the fullest treatment to the proto-sublayer in a porous medium, the other cases being very similar.

(*a*) *The proto-sublayer in a porous medium*

Let us consider the development of the proto-sublayer at the base of a slab of fluid saturated porous material. If we restrict our attention to the time interval during which the disturbances are sufficiently small to neglect quantities of second order in the disturbance amplitudes, the equations of motion are linear. If at $t = 0$ the disturbance amplitudes are zero and there are no temperature fluctuations permitted on the walls, no disturbances are possible† and we have the solution of (1): $\theta = \Theta(z)$; $\psi = 0$ where

$$\frac{\partial \Theta}{\partial t} = \Theta_{zz}. \tag{3}$$

This is the ordinary heat conduction equation (Carslaw & Jaeger 1959, §2.4) with the solution

$$\Theta = \operatorname{erfc}(z/d), \tag{4}$$

where

$$d = d(t) = 2\sqrt{t}.$$

If, however, at $t = 0$ the disturbance amplitudes are non-zero (say, for example, there are temperature fluctuations on the walls) we can write the temperature‡ as $(\Theta + \theta)$, where, neglecting $\partial(\psi, \theta)$ which for a range of t will be much less than $\nabla^2\theta$ or $\partial\theta/\partial t$, we have

$$\frac{\partial \theta}{\partial t} = \nabla^2\theta - \beta\psi_x. \tag{5}$$

Here

$$\beta = \beta(z,t) = \Theta_z = -(2/\pi d)\, e^{-(z/d)^2} \tag{6}$$

is the local vertical temperature gradient of the undisturbed temperature profile. In this approximation, all the heat from the wall continually accumulates in a horizontal layer and the growth of the temperature fluctuations is set by the net effect of thermal diffusion of the fluctuations and vertical advection by the vertical velocity fluctuations acting on the undisturbed temperature profile. Finally, since (1*a*) is a linear equation, with no approximation,

$$\nabla^2\psi = A\theta_x. \tag{7}$$

† This seems to me to be a trivial point, but is not generally as well appreciated as it should be. In the numerical experiments if $\epsilon = 0$ the solutions are those of (3).

‡ The use of θ here for the temperature fluctuation should not lead to confusion with θ used elsewhere.

(i) *The initial period of induced motion*†

If we consider the case in which the only source of noise is temperature fluctuations, so that at $t = 0$ we have $\psi = 0$, there will be a period of time during which $\beta\psi_x \ll \nabla^2\theta$. There is then no feedback from the velocity field to the temperature field and the flow is simply an induced one. In particular, this induced flow is independent of the growth of the mean temperature field. For the case in which the only source of temperature fluctuations is on the walls the induced motion is confined to a region near the wall. Each spectral component of the wall temperature fluctuations $\epsilon(x,t)$ is exponentially attenuated with depth of penetration into the fluid: a spectral component of ϵ of circular frequency ϖ penetrates the fluid to a depth of order $(2/\varpi)^{\frac{1}{2}}$ (Carslaw & Jaeger 1959, §2.6). In other words, because of the finite thermal diffusivity of the fluid, the noise at the wall passes into the fluid through a coarsely tuned low-pass filter. An example of such induced flow has been shown in figure 6.

(ii) *The period of gestation*

During the initial period the layer has been so thin as to be completely dominated by conduction, but as the layer grows we have the possibility of the increasing importance of the vertical advection of heat by the velocity fluctuations described by the term $-\beta\psi_x$. Hence from (5) and (7) we have $L\psi = L\theta = 0$ where

$$L = \left(\frac{\partial}{\partial t} - \nabla^2\right)\nabla^2 + \beta A \frac{\partial^2}{\partial x^2}. \tag{8}$$

Although we have a linear problem, a full treatment with $\beta = \beta(z,t)$ would be very complicated. The most complete analysis for the corresponding problem in a viscous fluid is that of Foster (1965*b*) who uses a spatial spectral representation of ψ and θ, the spectral amplitudes being time dependent.

The earlier analysis of Morton (1957) assumes $\partial\beta/\partial t = 0$ but the derivations, which are referred only to moderate values of A, have been questioned by Foster (1965*b*). The essence of what is done here follows from the observation in the laboratory and numerical experiments that the scales of the growing disturbances are those of the growing thermal layer.

Consider a possible spectral component:

$$\psi = \sin kx \sin mz\, \phi(t); \quad m/\pi = 1, 2, \ldots, \tag{9}$$

so that,

$$\left[\left(\frac{\partial}{\partial t} + k^2 + m^2\right)(k^2 + m^2) + \beta A k^2\right]\phi = 0. \tag{10}$$

Now it is clear, provided $(-\beta A)$ is sufficiently large, that $\phi_t > 0$ and amplification is possible. On the other hand, in regions where $(-\beta A)$ is small or zero, amplification is impossible and the only possible motions are damped. We therefore make the gross assumption that to a first approximation the growth rates can be

† In passing, it should be remarked that during this interval there is a somewhat similar period of adjustment in the numerical simulation, given by $2\sqrt{t} \approx d'$ where d' is the mesh spacing. For the data of figure 11 this time is about 10^{-4}. Beyond this time the induced flow is seen to be in (numerical) equilibrium with the noise source.

calculated by setting $\beta(z,t) = -1/\delta(t)$ for $0 \leqslant z \leqslant \delta(t)$ and $\beta(z,t) = 0$ for $z > \delta(t)$, where $\delta \equiv \alpha d$ and α is a fudge factor of $O(1)$ describing the net effect of non-uniformity of β. In addition, we assume that motion is restricted to the region $0 \leqslant z \leqslant \delta$. In other words, inspection of (10) shows us that amplification of a given spectral component is only possible in those parts of the field where $(-\beta A)$ is sufficiently large, so that we expect the motion to be largely confined to the region $0 \leqslant z \leqslant \delta$. Hence: for $z > \delta$ we have $\psi = \theta = 0$; for $0 \leqslant z \leqslant \delta$, (9) and (10) apply but we rewrite $m = \pi/\delta$ $(1, 2, 3, \ldots)$. Since the growth rate is largest for the smallest possible value of m we take $m = \pi/\delta$ henceforth. We note in passing that in the corresponding Rayleigh–Bénard type of problem, which determines the least value of A for which any motion is possible, we could put $\beta = -1$ with little error. This is Morton's (1957) principal result.

Let us first estimate the time at which amplification will commence, that is, *when at least one component can grow*. This is simply the classic stability problem of the Bénard–Rayleigh type which was first evaluated for flow in a porous medium by Horton & Rogers (1945) and Lapwood (1948). From (10),

$$(m^2+k^2)^2 = -\beta A k^2, \tag{11}$$

so that growth is first possible when $(-\beta A) = A_c = 4\pi^2$ for $m = k$. Hence, since $\delta = 2\alpha\sqrt{t}$ the critical time t_c is given by (see also Elder 1967*c*, §4),

$$t_c = (A_c/A)^2/4\alpha^2. \tag{12}$$

(iii) *Superexponential growth*

For $t > t_c$ amplification is possible. The analysis of the interval immediately after $t = t_c$ is difficult because $\beta_t \neq 0$. This is simply because since $n = 0$ at $t = t_c$ there will always be an interval in which the growth rate n is very small compared to the effects of β_t. We can, however, crudely understand the process by means of the following rather heuristic argument.

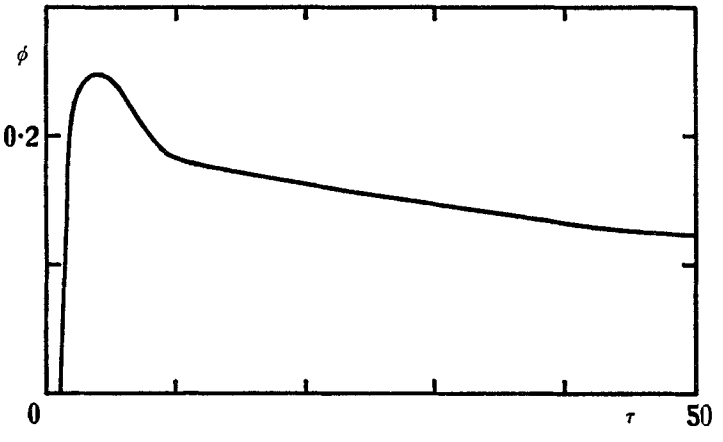

FIGURE 21. Variation of exponential growth rate n as a function of time given by (14*a*) for a proto-sublayer in a Hele-Shaw cell.

We notice that the first disturbance to be amplified satisfies $k = m$. Let us therefore assume that the dominant disturbance has $k = m$, at any time t im-

pose such a disturbance, and ask what its growth rate, $n \equiv \partial \log \phi / \partial t$ would be. Hence in (10) we write

$$k = m = \pi/\delta, \tag{13a}$$

so that

$$n = (A\delta - 4\pi^2)/2\delta^2. \tag{13b}$$

Writing $\tau = t/t_c$ so that $\delta = \delta_c \tau^{\frac{1}{2}}$ we have

$$n = \tfrac{1}{2}(A/A_c)^2 \phi_m(\tau), \tag{14a}$$

where

$$\phi_m = \tau^{-\frac{1}{2}} - \tau^{-1}. \tag{14b}$$

The form of $n(\tau)$ is sketched in figure 21. We notice that there is a very rapid increase of ϕ_m to a maximum of 0·25 at $\tau = 4$ (i.e. $\delta = 2\delta_c$) followed by a very gradual decrease. This result suggests that in an interval following the first appearance of amplification, growth is superexponential. This is a consequence of the growth of the mean profile. In Bénard–Rayleigh convection where the mean profile is time independent, growth rates are (initially) exponential, but here the effective Rayleigh number $A\delta^3 \propto t^{\frac{3}{2}}$ is also increasing.

(iv) *Quasi-equilibrium*

Beyond $\tau = 4$, as τ becomes larger the change in n over a given interval of time becomes smaller, so that provided A is sufficiently greater than A_c for n to be large the system behaves as if it were in quasi-equilibrium. Note in (13*b*) that as δ increases we have

$$n \sim \tfrac{1}{2}(1/\delta)A. \tag{15}$$

Now this result is precisely the same as that obtained by putting $\partial\beta/\partial t = 0$. If we had assumed $\partial\beta/\partial t = 0$ at the outset we would argue that in (11) if βA is large so that n is also large, we can neglect the term $(m^2 + k^2)$ in relation to n and obtain (15). The neglect of this term implies that the thermal diffusion of temperature disturbances is negligible.

It follows that during the period of superexponential growth the role of thermal diffusion has been progressively diminishing relative to that of the vertical advection of heat by the vertical velocity fluctuations acting on the mean temperature field. Also we see that the quasi-equilibrium state is only reached after the role of thermal diffusion has become negligible.

The result (15) has the form we would expect. Since

$$\beta = -1/\delta \quad \text{and} \quad A(\delta) = A\delta = A_c \tau^{\frac{1}{2}},$$

we have

$$n = \tfrac{1}{2}A^2/A_c\tau^{\frac{1}{2}}. \tag{16}$$

This result in *dimensional* form is independent of H as it must be if A is sufficiently large.

(v) *Birth and flight*

During the period of gestation the disturbance has been embedded in the proto-sublayer. That is to say the eddies only occupy a region of extent δ. But as the disturbance amplitudes become larger and θ becomes $O(1)$, gross distortions of the proto-sublayer temperature field become noticeable and the eddies begin to emerge from the layer. In the data of figure 11 this time is of order $2{\cdot}5 \times 10^{-3}$

during which time the disturbance streamfunction has been amplified by a factor of about 25. The layer is now dominated by the buoyancy forces and the eddies are accelerated out of the layer. Heat is transferred out of the layer by advection of the temperature fluctuations by the velocity fluctuations.

Linear analysis is no longer adequate during this eruptive phase. We can, however, make one further important deduction. The curved dotted line shown in figure 11, which is a line ψ_m/t = constant, suggests that the blobs are uniformly accelerated out of the layer. But in a porous medium the inertial accelerations play no role in the dynamics. Hence an explanation other than that of a free flight must be sought. If we can identify the mean temperature ϑ of a blob, then directly from the vertical momentum equation the mean vertical velocity $W = A\vartheta$. If $\partial W/\partial t \doteqdot$ constant, then $\partial\vartheta/\partial t \doteqdot$ constant. Hence during the initial period of blob production, fluid from progressively deeper in the sublayer must be entrained into the blob. This process locally thins the sublayer surrounding the blob and continues till the sublayer is largely denuded. The disturbance grows a further order of magnitude (in figure 11) in this interval. At this time the blob has become a discrete and separate entity and rises above the layer with nearly constant velocity. Thence the blob reacts with the ambient environment largely by entraining cold ambient fluid.

Thus the gravitational energy which has been accumulating in the sublayer during the gestation period is in this final phase rapidly entrained into the growing blobs *before* being released into the ambient fluid.

The problem of the rise of a buoyant element through fluid initially at rest has been studied by many people. For example there are the notable experimental studies of Turner (e.g. 1963) and the numerical work of Lilly (e.g. 1964, which has a good bibliography). As far as I am aware, these studies only consider the subsequent development of a given blob, and are not concerned with its origin. It is here that the present work is rather interesting for it reveals, at least in outline, the mechanism of accumulation of buoyancy in the blob and gives some idea of the process of eruption. The process of blob production is seen as gradual but inevitable. One wonders if a similar process of increasing dominance of entrainment over diffusion is responsible for the origin of buoyant elements, such as thermals, in the lower atmosphere.

(*b*) *The proto-sublayer in a viscous fluid*

The development of the proto-sublayer in a viscous fluid can be discussed in a similar manner. The only additional feature in the linearized equations is the term representing the diffusion of vorticity, the advection of vorticity being a term of second order. The secular equation for a single spectral component is now

$$[n+(m^2+k^2)][(n/\sigma)+(m^2+k^2)](m^2+k^2) = \beta A^* k^2. \tag{17}$$

For free boundaries, we have (Rayleigh 1916) $n = 0$ first for

$$(-\beta A^*) = A_c^* = 27\pi^4/4 \quad \text{and} \quad m = \sqrt{2}k.$$

Also the critical time

$$t_c = \frac{1}{4\alpha^2}(A_c^*/A^*)^{\frac{2}{3}} \tag{18}$$

and the growth rate for large A^* and $\sigma \approx 1$ is

$$n^2 \sim \tfrac{1}{3}\sigma(-\beta A^*). \tag{19}$$

Solutions for other values of σ are readily obtained from (17).† Both these results, in dimensional form, are independent of H.

During the superexponential period, as in the case of a porous medium we write in (17): $m^2 = 2k^2$; $m = \pi/\delta$; $\delta = \delta_c \tau^{\frac{1}{2}}$ and note that $A_c^* = \frac{27}{4}\pi^4 = A^*\delta_c^3$ so that for example in the case of $\sigma = 1$,

$$n \sim \frac{1}{\sqrt{3}} A_c^{*-\frac{1}{6}} A^{*\frac{2}{3}} \phi_\nu(\tau), \tag{20a}$$

where

$$\phi_\nu(\tau) = \frac{1}{\tau^{\frac{1}{4}}} - \frac{1}{\tau}. \tag{20b}$$

Thus $\phi_\nu(\tau)$ has the same qualitative form as (14*b*) in a porous medium.

(*c*) *The isolated thermal interface in a viscous fluid*

The form of the above expressions (15) and (19) for the growth rates is rather similar to that found in the simplest version of the Rayleigh–Taylor problem in which we consider the initial distortion of a sharp interface between two fluids when the upper fluid is denser than the lower fluid. If we can neglect both the diffusion of density and of vorticity we have the simple result of Rayleigh (1900), expressed in terms of our present units,

$$n^2 = \tfrac{1}{2}\sigma A^* k, \tag{21}$$

where as above k is the horizontal wave-number of the disturbance.‡ Strictly (21) applies only to two perfect immiscible fluids. For real fluids we must argue that provided the development of the instability is sufficiently rapid we can ignore the diffusion of density and vorticity. But this can never be true in the period immediately following $t = 0$, when the rate of diffusion across the interface is highest. However, during this period disturbances can also grow in the 'interface' itself. Now we see how the scale k of the interfacial distortion is determined! It is determined by the scale of the disturbances in the 'interface'. The expression (21) indicates that the most rapidly growing distortion of the interface is that with the smallest length scale. But the smallest length scale is the scale of the interface and since the dominant scale of the disturbance in the interface is that which grows most rapidly, that has a scale of order δ. The expressions (19) and (21) are indeed equivalent if we place $k = \frac{2}{3}/\delta$.

The numerical experiment presented in figure 20 clearly demonstrates that the initial growth of the interfacial distortions are set by δ and not by the other possible scales, namely, the scale of the initially imposed temperature fluctuations or of the distance h from the wall.

† Writing $n = yA^{\frac{2}{3}}/A_c^{\frac{1}{6}}$ and $p = 3\pi^2/2A_c^{\frac{1}{6}}$ we have $(y+p)([y/\sigma]+p) = \frac{1}{3}$. Note for $\sigma \to \infty$ we have $y \sim \frac{1}{3}p$ so that n is independent of σ.

‡ It would be ridiculous generally to write the result in this form, but in this paper we are interested in the combined role of κ and ν. The expression in dimensional form $n^{*2} = \frac{1}{2}gk\Delta\rho/\rho$ does not involve κ or ν. See also the paper by Bellman & Pennington (1954).

8. Comparison of results

It is of interest to compare the numerous results we have obtained. The essentially phenomenological models of §7 involve: the Rayleigh number, A or A^*; a fudge factor α which allows for the fact that the shape of the temperature profile is not linear; a critical Rayleigh number, A_c or A_c^*, which here, for want of a better choice, we take as the value given by the corresponding Bénard–Rayleigh problem; and a time-dependent function $\phi(\tau)$ which crudely represents the combined influences of growth of the temperature profile and growth of the disturbances. The latter three factors are not precisely predicted by the model of

	(i) Porous)		(ii) Viscous		(iii) Isolated		
A or A^*	400	800	10^6	10^7	10^6	10^7	Note
t_1	$1{\cdot}35\times10^{-3}$	$3{\cdot}5\times10^{-4}$	$1{\cdot}44\times10^{-3}$	$3{\cdot}1\times10^{-4}$	$7{\cdot}2\times10^{-4}$	$1{\cdot}8\times10^{-4}$	*a*
$\alpha^2 t_c$, §7	$2{\cdot}5\times10^{-3}$	$6{\cdot}25\times10^{-4}$	$2{\cdot}67\times10^{-3}$	$5{\cdot}7\times10^{-3}$	$1{\cdot}96\times10^{-3}$	$4{\cdot}2\times10^{-4}$	*b*
$1/\alpha^2$	0·54	0·56	0·54	0·55	0·37	0·43	*c*
n_{obs}	342	1610	680	3500	1140	4500	*a*
n/ϕ, §7	2000	8000	1800	8400	1960	9100	*b*
ϕ	0·17	0·20	0·38	0·42	0·58	0·50	*c*
$\phi_{\max}$	0·25		0·47		0·47		
A_c	40		1100		650		*d*

TABLE 1. Comparison of time scales, critical time t and exponential growth rate n, obtained by numerical experiment and the results of §7 for three flows: (i) porous medium; (ii) viscous fluid; (iii) isolated interface in a viscous fluid with $h = \frac{1}{2}$: at pairs of Rayleigh numbers, A. The fudge factor $\alpha \equiv d/2\sqrt{t}$. The maximum possible value of ϕ given in §7 and the value of A_c used are also shown. All these results are for a mesh spacing of 1/40 and a noise level of $\epsilon' = 0{\cdot}2$.

Note: *a*, numerical values; *b*, obtained from (14) or (20) using (*d*); *c*, (result *a*)/(result *b*).

§7 principally because of the crude representation of the temperature profile. Close comparison with the numerical experiments is therefore not to be expected. Nevertheless, all the results show sufficient consistency to suggest, provided that we use the numerically determined value of α, that extrapolation of these results, in particular to other Rayleigh numbers, will be correct to better than $\pm 20\%$. The correlation of the results is displayed in table 1, which shows data from six numerical experiments and the corresponding results from §7. The numerical values of t_1 can be found to about $\pm 10\%$ and n to about $\pm 5\%$. The choice of Rayleigh numbers is dictated by computer time and the need to represent adequately the interface spatially.

We would expect the role of A to be well represented as it is for the critical times and the growth rates. For example, the data of figure 12 show $n/A^2 \approx$ constant as required by (14). On this point our results for a viscous fluid are in close agreement with the data given by Foster (1965). The relation $t_c(A^*)$ estimated from Foster's figure 6 gives $\partial(\log t_c)/\partial(\log A^*) = -0{\cdot}68$ close to the above $-2/3$. His critical wave-number $k_c \propto A^{*\frac{1}{3}}$.

It is in the values of the numerical coefficients that the present results are uncertain. The fudge factor α which relates d and δ ($=\alpha d$) only affects here the value of t_c (and not n). Both the porous medium results and the viscous fluid results require $\alpha \approx 1{\cdot}35$. This is a not unreasonable value since at $z = 1{\cdot}35d$ from (6) we have $-\beta d = 0{\cdot}18$ so our approximation uses about 80% of the layer. The free interface requires $\alpha \approx 1{\cdot}6$, a somewhat larger value than for the interface on a wall.

The growth rate n obtained numerically only qualitatively follows $\phi(\tau)$. For example, the porous medium results give the asymptotic value $n/A^2 = 2{\cdot}5 \times 10^{-3}$ $\pm$ 15%. This is compatible with (14) and $A_c = 4\pi^2$ provided $\phi \approx 0{\cdot}2$. Inspection of figure 21 shows that $\phi \approx 0{\cdot}2$ when $\tau \approx 2$ or 8 but rises to 0·25 at $\tau = 4$. Typically the exponential region in the numerical experiments extends to $\tau \approx 4$. Hence our prediction is moderately correct but, if anything, something of an underestimate by as much as perhaps 20%. The viscous fluid data similarly requires $\phi \approx 0{\cdot}4$ compared with the maximum possible value of 0·47. The values of ϕ required for the isolated interface are rather higher than $\phi_{\max}$. The difference is not very large but suggests that A_c^*, which we have taken to be 650 for a free interface, is somewhat less and from (19) is more like 100. This seems to me unreasonably low and is not compatible with the t_1 data.

It is worth noting that here the asymptotic growth rate obtained as $\tau \to \infty$, that is when for example in (20) $\tau^{-\frac{1}{4}} \gg \tau^{-1}$, occurs at values of τ large compared with the time to disrupt the layer. Hence estimates of growth rates in flows of the above type based on results asymptotic in time should be used with caution.

One feature of the analysis which has not been explicitly checked is the relation of the various time scales to A_c as indicated in (12), (14), etc. This is an important matter since, when other stabilizing processes are present, such as an imposed magnetic field if the fluid is an electrical conductor or the thermal diffusivity is a rapidly increasing function of temperature due to the diffusion of photons, the thermal layer will be considerably thicker before instability sets in. The total energy stored in the thermal layer is correspondingly higher and there is the possibility that the ultimate disruption of the layer will be more violent.

9. Some speculations about thermal turbulence

The present results permit us to make a number of comments on the role of the thermal sublayer in thermal turbulence.

The object of our study, the growth of disturbances in a thin thermal layer, can be considered as a problem in its own right, quite independently of the problem of the sublayer in fully developed turbulence. Indeed, this is how the work is presented. Clearly, the relation of these results to the problem of thermal turbulence must await a detailed study of the evolution of fully developed thermal turbulence and in particular of the evolution of the frequency and spatial spectra. Nevertheless, visualizations of the temperature and velocity fields in and near the sublayer (Elder 1967*a*) reveal that the major heat transfer process—blobs accelerated out of the sublayer—is the same in the initial, proto-sublayer phase

and in the fully developed state. At first sight this is somewhat surprising because in the initial phase the ambient fluid is at rest (and at uniform temperature), whereas in the mature state the ambient fluid is in vigorous motion. In the mature state the dominant scales of motion correspond to the largest eddies, of typical dimension H, the fluid depth. Hence the ambient fluid near the sublayer, apart from sites of convergence and divergence, is largely a horizontally flowing stream. We therefore ask the question, does the presence of this stream affect the growth of disturbances in the sublayer? A partial answer to this question has been given for the case of an *imposed* horizontal velocity field on the sublayer. If a typical velocity of the horizontal stream is U we have the additional parameter UH/κ, the Peclét number. In the author's study (Elder 1967*c*), over the range of Peclét numbers 0–10^3, no qualitative changes were found in the blob production of the sublayer. This of course does not answer the question, for we must also investigate the role of ambient shear and ambient vertical temperature gradients (to be published separately) especially those produced by a field of large eddies. In my view, therefore, this investigation forms one of a possible sequence of studies each of which attempts to analyse a particular aspect of a field of thermal turbulence.

There are other considerations on the theoretical side which indicate the relevance of this work to the thermal turbulence problem. Spiegel (1965), in a delightful paper, emphasizes the success of what he calls the weak-coupling approximation in which the only non-linear term retained in the analysis is that representing the vertical flux of heat produced by the vertical velocity fluctuations working on the horizontal mean vertical temperature gradient. He refers especially to the detailed studies of Herring (1963, 1964). Clearly the reason this approximation works as well as it does is that, provided the Prandtl number is not too small, the mean temperature gradients are only large near the horizontal boundaries. Hence the mean temperature change across the bulk of the flow is very small and a very crude representation of the non-linear fluctuating quantities, even putting them to zero, cannot affect the essential features of the flow.

In his pioneering theory Malkus (1954) had emphasized the marginal stability character of the sublayer. This idea is further developed in Howard's (1964) view of the intermittent growth and denudation of the sublayer. If we accept Howard's point of view, together with the qualitative laboratory observations of the similarity of the sublayer and the proto-sublayer, it is plausible that the processes discussed in §7 are those responsible for the maintenance of the sublayer.

Finally, the discussion of §7 suggests an explanation of one hitherto rather puzzling fact. Various experimenters report quite different values of the Rayleigh number at which the flow is 'turbulent'. Even allowing for the different ways of identifying the turbulent state can hardly explain the wide reported range of 10^4–10^8. The only possible cause that comes to mind is the effect of possibly different noise sources on the boundaries. With this in mind let us therefore attempt to write down a criterion for the occurrence of thermal turbulence. We take as our model that indicated at the end of §2, namely a field of large eddies with sublayers on the wall. Let us make the hypothesis that thermal turbulence will not be

possible unless a disturbance growing in the sublayer, and being swept along by the large eddy field, grows sufficiently to produce a blob. The longest time a disturbance will have to grow is set therefore by the time to travel a horizontal distance of $O(1)$, the horizontal large eddy scale, in the velocity field of a large eddy whose velocities† are $KA^{\frac{1}{2}}$ where $K = O(1)$. Hence the time a disturbance has to grow is no more than

$$t_g \sim 1/KA^{\frac{1}{2}}. \tag{22}$$

During this time the disturbance grows to an amplitude determined by $\tau = t_g/t_c$ and the noise input ϵ' where t_c is given by (18). Thus blobs appear in the sublayer provided $\tau = \tau(\epsilon')$ is sufficiently large, that is for

$$A > A_t = (0{\cdot}25K)^6 \tau^6 A_c^4. \tag{23}$$

We see how very sensitive A_t is to τ and therefore to ϵ'.

This argument can be put another way. What we are really saying is that the motion will be turbulent if the time of development of disturbances in the sublayer is shorter than the orbit time of the large eddies. If this is the case, the large eddies and the sublayer become decoupled and to a degree behave independently. This idea of a range of weakly coupled motions of different scales is a well known one in turbulence theory.

We begin to see a little more clearly one of the problems facing the analyst in developing a complete dynamical theory of thermal turbulence. The peculiar behaviour of the sublayer, seen here as a low pass filter whose cut-off frequency is increased as the disturbance grows only to be reduced again after the blob is released, must be included in any such theory. For the moment it seems to me to be more revealing to develop simple phenomenological descriptions of isolated features of the flow.

The numerical studies were performed with the author's programming system *Knees* on the University of Cambridge Mathematical Laboratory's *Titan*. I am most grateful for the use of this excellent facility. The apparatus was constructed by Mr David Cheesley. The work was supported by the British Admiralty and a grant from IBM (United Kingdom).

REFERENCES

BELLMAN, R. & PENNINGTON, R. H. 1954 *Quart. Appl. Maths*, **12**, 151.

CARSLAW, H. S. & JAEGER, J. C. 1959 *Conduction of Heat in Solids*. Oxford: Clarendon Press.

CHANDRASEKHAR, S. 1961 *Hydrodynamic and Hydromagnetic Stability*. Oxford: Clarendon Press.

DEARDORFF, J. W. & WILLIS, G. E. 1965 *J. Fluid Mech.* **23**, 337.

ELDER, J. W. 1967*a* In *The Mantles of the Earth and Terrestrial Planets*, p. 525. Ed. S. K. Runcorn. New York: Wiley.

ELDER, J. W. 1967*b* *Physics of Fluids* **10**, *Suppl.* S 237.

ELDER, J. W. 1967*c* *J. Fluid Mech.* **27**, 609.

† The $A^{\frac{1}{2}}$ dependence strictly applies to steady laminar flow, but is appropriate here since the result (23), with this model, is in effect a necessary condition for the flow to remain laminar.

FOSTER, T. D. 1965*a* *Phys. Fluids*, **8**, 1770.
FOSTER, T. D. 1965*b* *Phys. Fluids*, **9**, 1249.
HERRING, J. 1963 *J. Atm. Sci.* **20**, 325.
HERRING, J. 1964 *J. Atm. Sci.* **21**, 277.
HORTON, C. W. & ROGERS, F. T. 1945 *J. Appl. Phys.* **16**, 367.
HOWARD, L. N. 1964 *Proc. 11th Int. Congr. Appl. Mech.* Berlin: Springer-Verlag.
LAPWOOD, E. R. 1948 *Proc. Camb. Phil. Soc.* **44**, 508.
LILLY, D. K. 1964 *J. Atm. Sci.* **21**, 83.
MALKUS, W. V. R. 1954 *Proc. Roy. Soc.* A, **225**, 196.
MORTON, B. R. 1957 *Quart. J. Mech. Appl. Math.* **10**, 433.
RAYLEIGH, LORD 1900 *Scientific Papers*, ii, 200. Cambridge University Press.
RAYLEIGH, LORD 1916 *Scientific Papers*, **6**, 432. Cambridge University Press.
SPANGENBERG, W. G. & ROWLAND, W. R. 1961 *Phys. Fluids*, **4**, 743.
SPIEGEL, E. A. 1965 *Proc. 5th Cosmical Gas Dynamics Symposium, Nice.*
TURNER, J. S. 1963 *Quart. J. Roy. Met. Soc.* **89**, 62.
WOODING, R. A. 1957 *J. Fluid Mech.* **2**, 273.

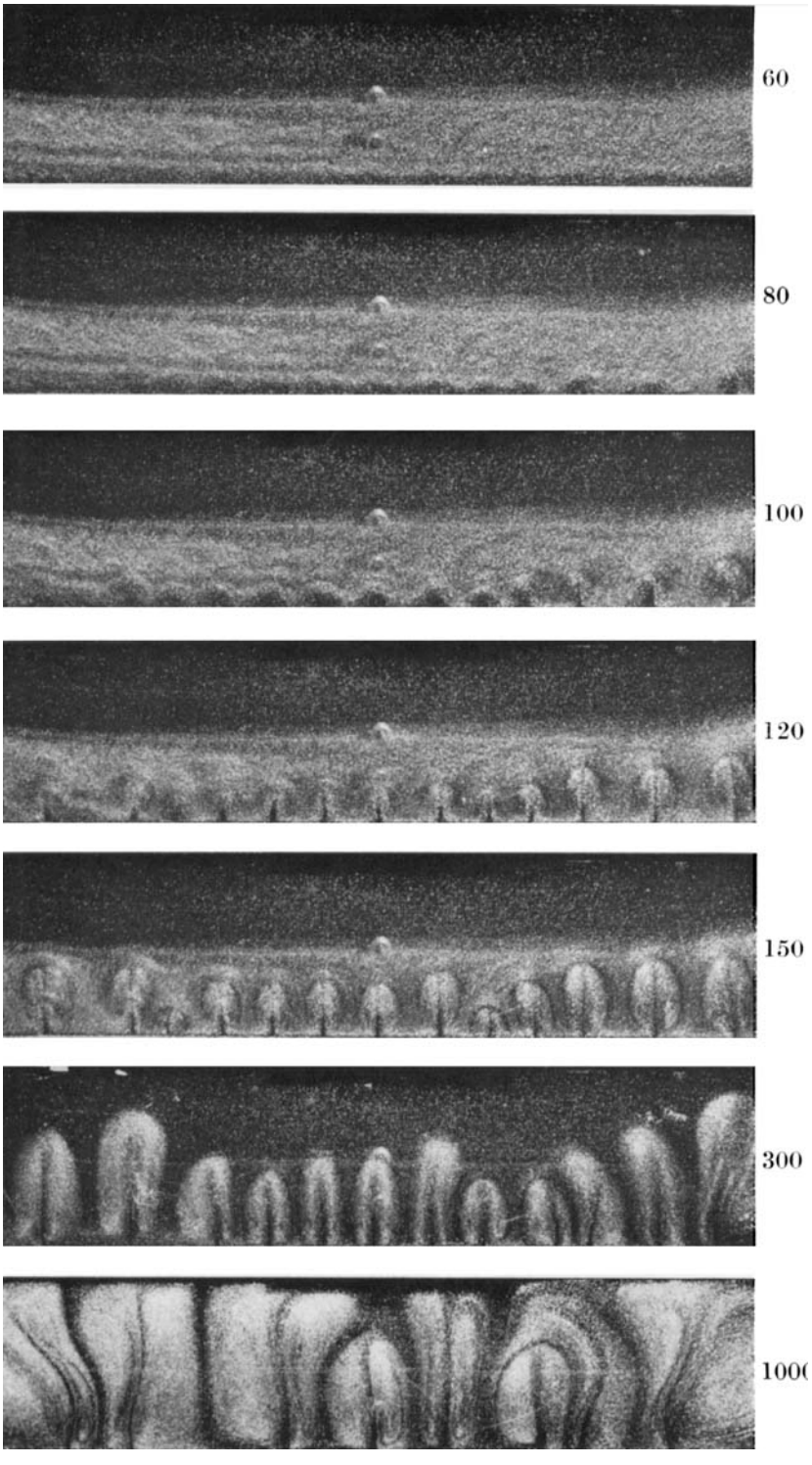

FIGURE 3. Photographic sequence of the development of high Rayleigh number flow in a Hele-Shaw cell. A full view showing a 16 cm width of a 4 cm deep layer. The numbers are the times in seconds after suddenly elevating the temperature of the bottom of the layer. The first motion is observed at about 60 sec. Fluid, silicon oil MS 200/100 cs; $A = 250$. The two circular patches of light, 1 and 2 cm above the base are thermocouple fittings seen through the rear wall of the cell.

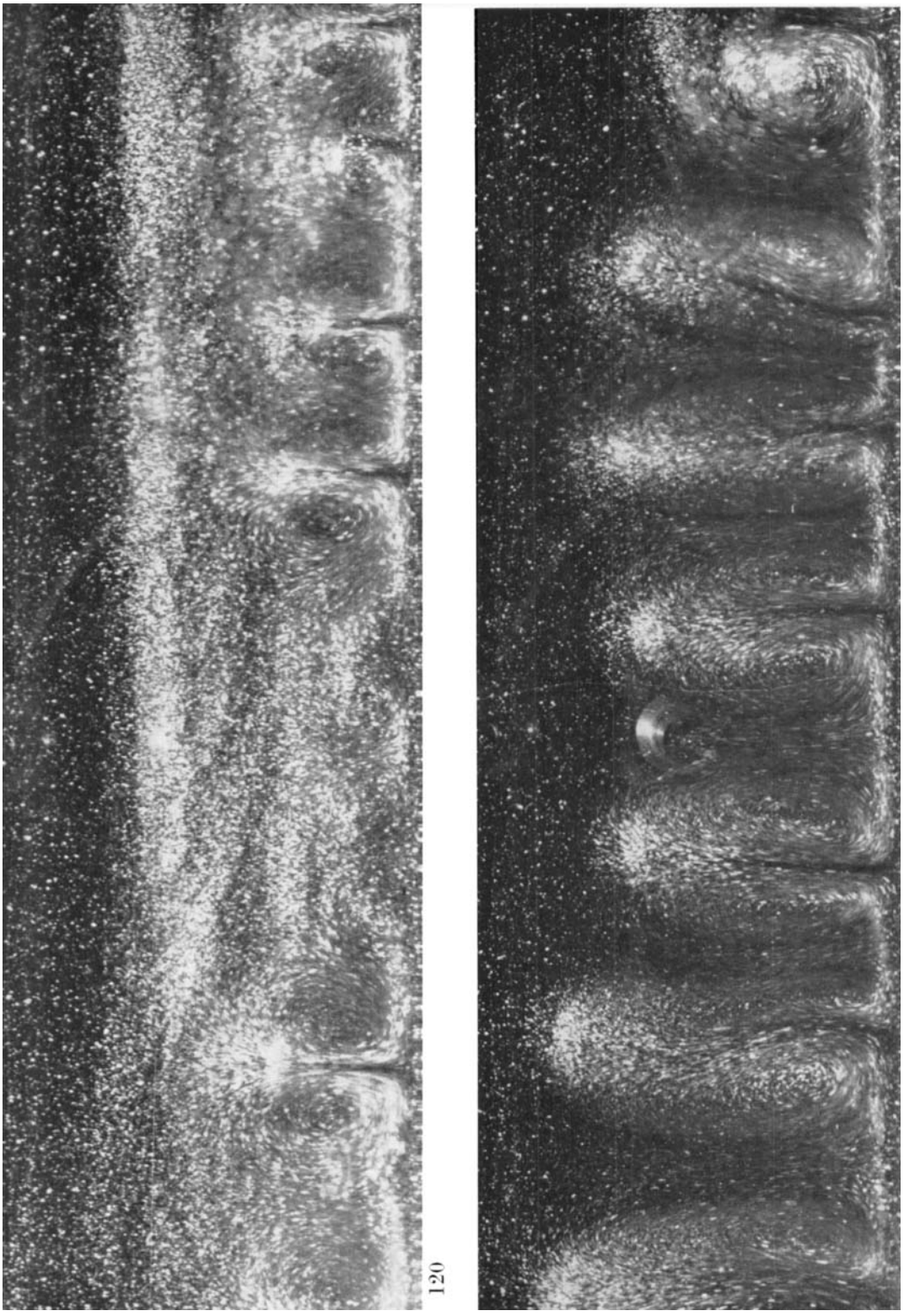

FIGURE 4. Photographic sequence of the development of the thermal interface near a wall. As in figure 3 but only showing the protolayer in the lower 2 cm of the fluid layer.